Flowing water enabled piezoelectric potential of flexible composite film for enhanced photocatalytic performance

Baoying Dai, Hengming Huang, Fulei Wang, Chunhua Lu, Jiahui Kou, Lianzhou Wang, Zhongzi Xu

PII: S1385-8947(18)30574-6
DOI: https://doi.org/10.1016/j.cej.2018.04.008
Reference: CEJ 18808

To appear in: *Chemical Engineering Journal*

Received Date: 14 December 2017
Revised Date: 7 March 2018
Accepted Date: 4 April 2018

Please cite this article as: B. Dai, H. Huang, F. Wang, C. Lu, J. Kou, L. Wang, Z. Xu, Flowing water enabled piezoelectric potential of flexible composite film for enhanced photocatalytic performance, *Chemical Engineering Journal* (2018), doi: https://doi.org/10.1016/j.cej.2018.04.008

Flowing water enabled piezoelectric potential of flexible composite film for enhanced photocatalytic performance

Baoying Dai[a,b,c], Hengming Huang[a,b,c,d], Fulei Wang[e], Chunhua Lu[a,b,c*], Jiahui Kou[a,b,c*], Lianzhou Wang[d], Zhongzi Xu[a,b,c]

[a] State Key Laboratory of Materials-Oriented Chemical Engineering, College of Materials Science and Engineering, Nanjing Tech University, Nanjing, 210009, P. R. China.

[b] Jiangsu Collaborative Innovation Center for Advanced Inorganic Function Composites, Nanjing Tech University, Nanjing, 210009, P. R. China.

[c] Jiangsu National Synergetic Innovation Center for Advanced Materials (SICAM), Nanjing Tech University, Nanjing, 210009, P. R. China.

[d] Nanomaterials Centre, School of Chemical Engineering and Australian Institute for Bioengineering and Nanotechnology, University of Queensland, Brisbane, Queensland, 4072, Australia.

[e] State Key Laboratory of Crystal Materials, Shandong University, Jinan, 250100, P. R. China.

Corresponding Author

* Prof. Chunhua Lu (E-mail: chhlu@njtech.edu.cn, Tel: (+86)025-83587252).

* Associate Prof. Jiahui kou (E-mail: jhkou@njtech.edu.cn).

Abstract

Fast charge transfer and low recombination rate are two vital requirements to achieve high photocatalytic activity. In this work, we report the conversion of flowing water energy to piezoelectric potential on a new type of flexible composite film PVDF-$Na_{0.5}Bi_{0.5}TiO_3$-$BiOCl_{0.5}Br_{0.5}$ (PV-N-B) containing PVDF-$Na_{0.5}Bi_{0.5}TiO_3$ (PV-N) substrate and $BiOCl_{0.5}Br_{0.5}$, which significantly boosts the charge transfer of the photocatalytic composite film, resulting in improved photocatalytic capability by 2.33 times. The role of piezoelectric potential in photocatalysis process has been discussed in detail and the results reveal that higher potential output is more beneficial for photocatalytic performance enhancement. Moreover, the photocatalytic degradation intermediates of tetracycline (TC) over PV-N-B were detected by liquid chromatography-mass spectrometer and the possible photodegradation pathway of TC

has been reasonably proposed. It is verified that superoxide radicals are the main active species for PV-N-B to degrade TC. The durability experiments demonstrate the good stability of flexible composite film PV-N-B. In a wider perspective, this work provides an efficient flexible composite film, with great capability in converting flowing water energy into piezoelectric potential and improving photocatalytic activity, to bring the environmental pollution under control.

Keywords: photocatalysis, flowing water, piezoelectric potential, PVDF, $BiOCl_{0.5}Br_{0.5}$

1. Introduction

Owing to the increasingly severe environmental issues, photocatalysis technology has attracted more and more attentions, which possesses wide applications in purifying environment in a friendly and sustainable way [1, 2]. Plenty of photocatalysts have been reported to exhibit photocatalytic degradation ability to reduce or eliminate environmental containments, such as TiO_2, ZnO, BiOI, $NaBiO_3$, WO_3/BiOCl, BiOBr and so on [3-9]. Nevertheless, their photocatalytic activities are not good enough to satisfy the requirements of practical application because photogenerated electrons and holes could be recombined once again in the path of random separation. Lately, piezoelectric potential has been employed to enhance photocatalytic performance due to its capability in promoting spatial directed charge separation and accelerating charge transfer [10-16]. Although the photocatalytic activity can be improved, piezoelectric potentials are normally introduced by ultrasonic wave vibration, consuming massive energy. Hence, in the view of real

application, it is of great significance to utilize clean and renewable energy in nature to efficiently generate piezoelectric potential and thereby promote photocatalytic activity.

As is well known, green and sustainable energy, such as solar energy, wind energy, hydro-energy, hydrogen energy and geothermal energy, has attracted worldwide interests because of the energy crisis and catastrophic global warming in the modern world [17-23]. Among the abovementioned energy forms, flowing water, a kind of hydro-energy available in oceans, lakes, rivers and streams, is one of stable, continuous and accessible energy to generate electric energy in nature [24]. However, due to the mild energy output of flowing water, excellent flexibility and piezoelectric property are two essential factors for piezoelectric materials to generate considerate piezoelectric potential. Although inorganic piezoelectric materials exhibit higher piezoelectric coupling coefficient than organic ones, it is difficult for them to readily deform as it is driven by mild force. Whereas, organic piezoelectric materials possess superb flexibility, corrosion resistance, low cost, and environmentally friendly properties, which endows them with more advantages than inorganic ones to convert mild energy to piezoelectric potential [25-27]. Poly(vinylidene fluoride) (PVDF) is a typical organic piezoelectric generator, which has been extensively employed to generate piezoelectric potential [28-31]. Moreover, in our previous work, PVDF was used as photocatalyst film substrate to generate piezoelectric potential, playing a generic role in photocatalytic activity improvement [32]. It is reported that the piezoelectric performance of PVDF could be further enhanced by combination with

inorganic ferroelectric particles [33]. Therefore, flowing water may be converted to piezoelectric potential by modified PVDF film substrate, enhancing photocatalytic performance.

Hence, in this work, we report the design of a new type of flexible composite film PV-N-B, which could convert flowing water to piezoelectric potential and dramatically boosts its photocatalytic efficiency. The piezoelectric properties of PV-N substrate and their effect on the photocatalytic property were studied in detail via piezoelectric force microscopy, photocatalytic degradation of TC, etc. Furthermore, the intermediates and possible photodegradation pathway of TC were studied. The active species for PV-N-B to degrade TC and the stability of PV-N-B composite film were also investigated.

2. Experimental

2.1. Materials

Poly(vinylidene fluoride) ($(CH_2CF_2)_n$, PVDF, MW ~ 543000, Aldrich) and poly(dimethylsiloxane) ($(C_2H_6OSi)_n$, PDMS, Sylgard 184) and its curing agent from Dow Corning were used to prepare film substrates. N,N-Dimethylformamide (C_3H_7NO, 99.5%, Sinopharm Chemical Reagent Co., Ltd.) and xylene (C_8H_{10}, 99.0%, Shanghai Lingfeng Chemical Reagent Co., Ltd.) were used as the solvents of PVDF and PDMS, respectively. $BiOCl_{0.5}Br_{0.5}$ (Fig.S1, S2) and $Na_{0.5}Bi_{0.5}TiO_3$ (Fig. S3) were prepared in our experiment, respectively. All the reagents were of analytical grade and all the reagents were used without future purification. Distilled water was used in the whole experiment. The prepared samples and their corresponding abbreviations are

listed in Table. 1.

2.2. Fabrication of piezoelectric film substrates

PV-N: As Fig. 1 depicts, 1.0 g of as-prepared N nanosphere (Fig. S3) and 1.0 g of poly(vinylidene fluoride) powders were dispersed completely in 9.0 g of N, N-dimethylformamide by continuous stirring for 3 h. Subsequently, the obtained mixture was spin-coated on glass slides (2.5 cm × 7.6 cm) with a coating machine after scattered by ultrasonic wave for 10 min. At last, PV-N films with the thickness of approximately 100 μm were prepared after cured at 60 ^{o}C in a vacuum oven for 30 min. Pure PV films were also prepared via the fabrication process of PV-N in the absence of N powders.

PD-N: The preparation process of PD-N film is like that of PV-N. As-synthesized N, xylene, poly(dimethylsiloxane) and its curing agent (1:4:6:0.6 by weight) were mixed under ultrasonic wave irradiation for 10 min and strong stirring for 30 min to form homogeneous solution. After that, the mixture was spin-coated on glass slides (2.5 cm × 7.6 cm) with a coating machine and cured at 70 ^{o}C for 2 h in an oven. Finally, PD-N films with the thickness of about 100 μm were obtained. For comparison, pure PD films were fabricated as well.

Table. 1 The prepared samples and their corresponding abbreviations (abb.).

Sample	Abb.
$BiOCl_{0.5}Br_{0.5}$	B
$Na_{0.5}Bi_{0.5}TiO_3$	N
PDMS	PD
PDMS-$BiOCl_{0.5}Br_{0.5}$	PD-B
PDMS-$Na_{0.5}Bi_{0.5}TiO_3$	PD-N
PDMS-$Na_{0.5}Bi_{0.5}TiO_3$-$BiOCl_{0.5}Br_{0.5}$	PD-N-B
PVDF	PV
PVDF- $BiOCl_{0.5}Br_{0.5}$	PV-B
PVDF-$Na_{0.5}Bi_{0.5}TiO_3$	PV-N
PVDF-$Na_{0.5}Bi_{0.5}TiO_3$-$BiOCl_{0.5}Br_{0.5}$	PV-N-B

2.3. Preparation of photocatalytic composite films

PV-N-B: As Fig. 1 illustrates, three pieces of fabricated PV-N films were put into the precursor solution of B (supplemental materials) after plasma discharge treatment, which modifies the surface structures and wettability of PV-N substrates. The treatment of plasma discharge allows the reactive ions of photocatalyst to assemble and grow on the surfaces of film substrates. After continuous stirring for 12 h, the obtained PV-N-B composite films were washed with distilled water and ethanol for several times. For comparison, PV-B, PD-B and PD-N-B photocatalytic composite films were prepared as well in a similar way as that of PV-N-B except PV-N substrates were replaced by PV, PD and PD-N, respectively.

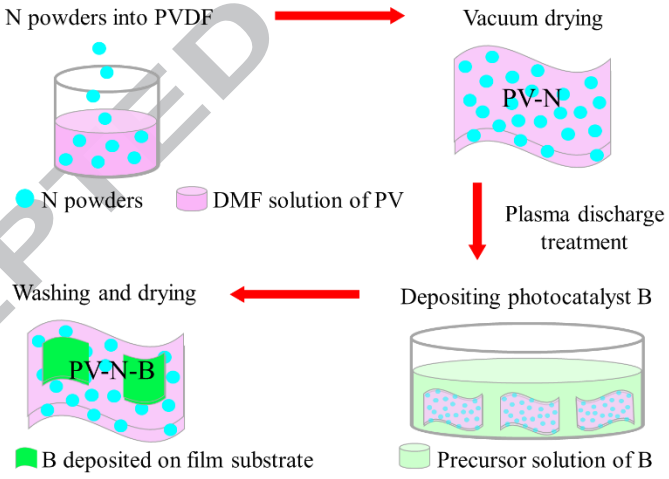

Fig. 1 Preparation procedures of PV-N and PV-N-B films.

2.4. Characterizations

The phase structure characterization of as-prepared samples was performed on a SmartLab (Rigaku) thin-film diffractometer employing Cu K_α radiation (λ=0.15406 nm), with a scanning rate of 10 °/min. The chemical states of photocatalyst B were characterized by X-ray photoelectron spectroscopy (XPS) in ESCALAB 250Xi with a

monochromatic Al Kα source (hν=1486.6 eV). All the binding energies were calibrated using the C 1s peak (BE=284.8 eV) as standard. Scanning electron microscopy (SEM) was performed with a S-4800 scanning electron analyzer with an accelerating voltage of 15 kV. Transmission electron microscopy (TEM) and high-resolution transmission electron microscopy (HRTEM) were acquired with a 200 kV FEI Tecnai. UV-vis diffuse reflection spectra were obtained using an ultraviolet-visible-near infrared (UV-Vis-Nir) 3101 spectrophotometer (Shimadzu) with $BaSO_4$ as the reflectance sample in the wavelength ranged from 200 nm to 800 nm. The absorption spectra were converted from reflection by Kubelka-Munk method. Piezoelectric force microscopy (PFM) images were carried out using a Bruker Dimension Icon Scanning Probe Microscope with a Pt-coated conductive tip. The piezoelectric potential output signals were collected with oscilloscope (Tektronix, TBS1102). Before characterization, 1 cm^2 of top and bottom surfaces of film substrates were sprayed with Au (conductive layer), two copper wires were used as conductive wires to connect Au layers to the positive and negative electrodes of oscilloscope, respectively.

2.5. Photocatalytic activity evaluation

A 300 W xenon lamp was used as light source, which irradiated at a distance of 20 cm to the reacting substance. The degradation of TC (10 mg/L, 100 mL) over the prepared samples were performed under magnetic stirring in the presence (MS-L) and absence (MS-NL) of light irradiation. As a contrast, the photodegradation experiments of TC were also carried out in the condition of light illumination with no stirring

(NS-L). Prior to catalytic reaction, three pieces of composite film were cut into six equal parts, strung together with copper wire and immersed in TC solution (Fig. 2) with magnetic stirring in dark to establish adsorption-desorption equilibrium. Photocatalytic activity evaluation system, conducted in the condition of MS-L, simulates the photocatalytic degradation process in nature, which allows the films to deform as water flows. During the test process, 3 mL of sample solution was taken out every 15 min and analyzed with a UV-Vis-Nir 3101 spectrophotometer. The concentration of TC was measured at its maximum absorption peak (λ=357 nm). The percentage of degradation is designated as C/C_0 (C and C_0 are the test and original concentration of the measured solution, respectively). The durability experiments of PV-N-B were conducted under MS-L.

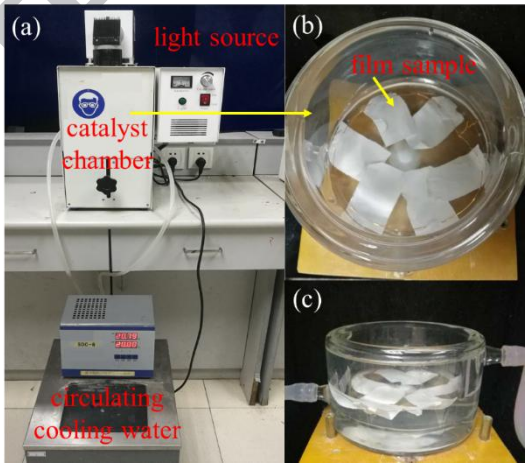

Fig. 2 Digital photograph of catalyst system used in the experiment (a), the top (b) and lateral (c) photographs of film sample located in reactor during photocatalytic process.

2.6. Intermediates and degradation pathway of TC analysis

The intermediates of TC over PV-N-B during photocatalytic degradation were identified by high performance liquid chromatography (HPLC, Shimadzu) and liquid

chromatography-mass spectrometer (LC-MS, Agilent 6540 Q-TOF). HPLC were equipped with C18 column of Shimazu Inersustain C18 (250*4.6 mm, 5 um) and a UV detector with the wavelength of 280 nm. The parameters for chloramphenicol analysis were set as follows: acetic acid, ultrapure water (75:25, v/v) and 5% methanol were employed as mobile phase, the flow rate of mobile phase was 0.5 mL/min, the sample injection volume was 10 μL and the chromatographic column temperature was kept at 40 ^{o}C. The mobile phase for LC-MS analysis was composed by methanol (80%) and ultrapure water (20%), the flow rate was set at 0.2 mL/min. 1 μL of sample solution was injected into LC system and the column temperature was kept at 40 ^{o}C. MS was carried out by operating in the positive ionization mode using dual ESI over the full scan acquisition of m/z ranged from 100 to 500. The spray voltage was set at 4 kV, the ion-transfer capillary temperature was 300 ^{o}C, the nebulizer and sheath gas flow rates were 35 arbitrary unit with an argon pressure of 0.2 MPa.

2.7. Active species trapping

Active species trapping experiments of PV-N-B were carried out under MS-L. 1 mM triethanolamine (TEA), 1 mM chromium (Ⅵ, Cr), 1 mM 1,4-benzoquinone (BQ) and 1 mM isopropanol (IPA) were employed as scavengers for h^{+}, e^{-}, $\cdot O^{2-}$ and $\cdot OH^{-}$, respectively. In active species trapping experiments, TC solution was replaced by the mixed solution composed of 10 mg/L TC and 1 mM scavenger. During the test process, 3 mL of the sample solution was taken out every 20 min and analyzed with UV-Vis-Nir 3101 spectrophotometer.

3. Results and discussion

The XRD patterns of the as-prepared samples are shown in Fig. 3. As Fig. 3 (a) displays, a broad diffraction peak presented at about 11.8 ^{o} of PD is the characteristic peak of poly(dimethylsiloxane). The XRD patterns of PD-B and PD-N are similar to that of pure PD film substrate except one weak peak of B and some typical diffraction peaks of N, which is ascribed to the small amounts of B depositing on the surfaces of PD substrate and the slight amounts of N contained in PD-N, respectively. All the peaks of PD-N-B can be indexed to that of B, N and PD. The peak of PV detected at approximately 20.6 ^{o} is indexed to β phase, depicted in Fig. 3 (b). It provides a demonstration that the β phase of PV is formed through the low-temperature synthesis process, indicating the piezoelectric property of prepared PV film [34, 35]. Furthermore, not only the peaks of B and/or N appear on the XRD patterns of PV-B, PV-N and PV-N-B, respectively, but also the diffraction peak of PV occurs on the XRD patterns of the above three films. It implies that the piezoelectric phase of PV preserves well after combined with B and/or N.

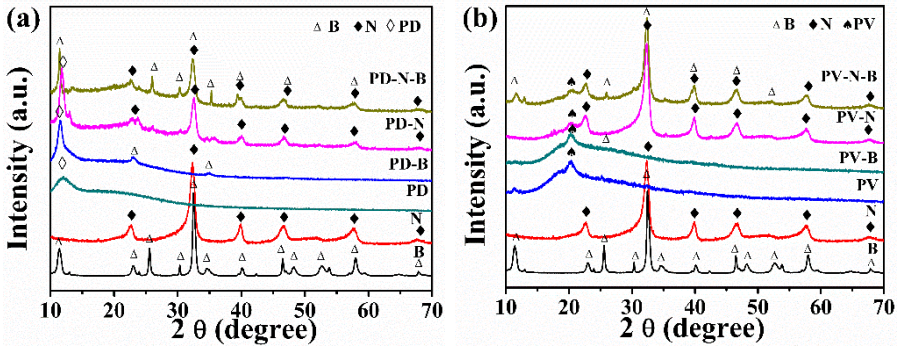

Fig. 3 XRD patterns of the as-prepare samples: B and N powders, PD, PD-B, PD-N and PD-N-B films (a); B and N powders, PV, PV-B, PV-N and PV-N-B films (b).

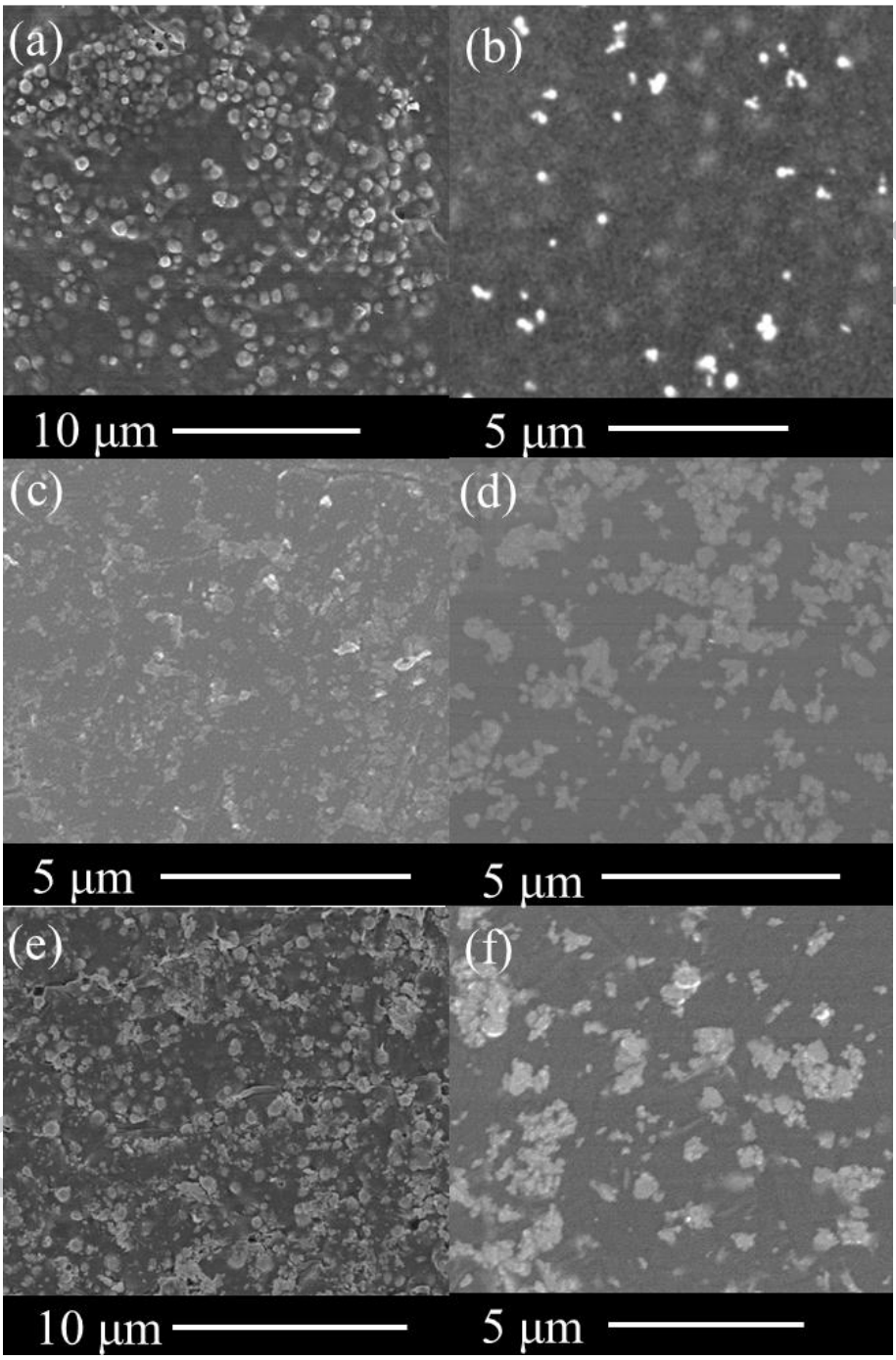

Fig. 4 SEM images of prepared composite films: PV-N (a), PD-N (b), PV-B (c), PD-B (d), PV-N-B (e) and PD-N-B (f).

The morphologies of the fabricated composite films were studied, shown in Fig. 4. Many of N particles distribute inside the bulk of PV and PD substrates, and the rest of particles are exposed on the surfaces of PV and PD, respectively (Fig. 4 (a) and Fig. 4

(b)). The SEM images of PV-B, PD-B, PV-N-B and PD-N-B films are presented in Fig. 4 (c), (d), (e) and (f), respectively. It can be found that the dispersiveness of B on PD and PD-N is not as good as that on PV and PV-N, respectively.

The UV-vis absorption spectra of the fabricated powders and films are displayed in Fig. 5. Pure PV and PD substrates exhibit continuous light absorption in the wavelength ranged from 200 nm to 800 nm. The absorption spectra of B, N, PD-N, PV-N, PD-B, PV-B, PD-N-B and PV-N-B films almost overlap with each other, starting at approximately 400 nm, which is responsive to visible light. It means that the existence of PV and PD does not play a negative role in the light absorption of prepared composite films.

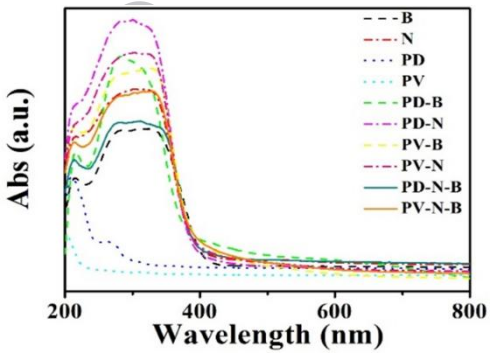

Fig. 5 UV-vis absorption spectra of the as-prepare samples: B and N powders, PD, PD-B, PD-N, PD-N-B, PV, PV-B, PV-N and PV-N-B films.

In order to penetrate a deep insight of the piezoelectric performance of prepared piezoelectric film substrates, the piezoelectric hysteresis and butterfly loops of PV, PD-N and PV-N were measured by PFM. Fig. 6 (a), (b), (c) and (d) depict the phase-tip bias and amplitude-tip bias loops of PV and PD-N substrates, respectively. No typical square phase hysteresis loops and butterfly loops are detected, which confirms the inferior piezoresponses of PV and PD-N substrates, respectively. The

obvious square phase hysteresis loop (Fig. 6 (e)) and the clear "butterfly shape" amplitude loop (Fig. 6 (f)) of PV-N suggest the characteristic piezoresponses with ferroelectric domain structures and distinct polarization switching behaviors of the film, respectively. Moreover, the phase reversal over PV-N is close to 180 ^{o} when the applied voltage is reversed from +12 V to -12 V (Fig. 6 (e)). It once more suggests the existence of 180 ° domains in PV-N and a distinct polarization switching process [36]. The amplitude butterfly loop of PV-N shifts to a positive voltage, implying the presence of internal electric field inside the film substrate PV-N (Fig. 6 (f)) [37]. The results demonstrate that the attendance of N inside PV endows the film substrate with superior ferroelectric property.

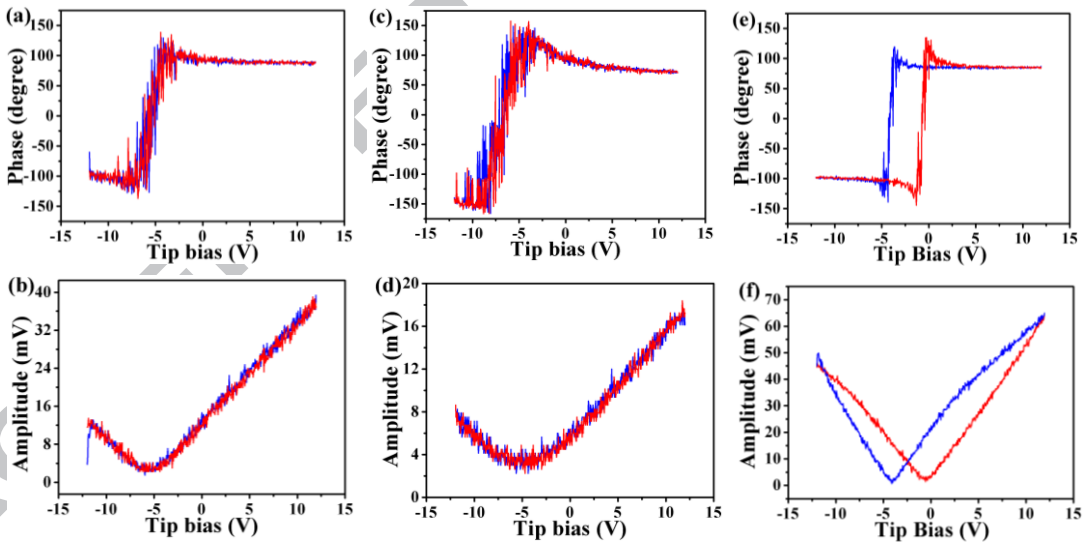

Fig. 6 Piezoelectric hysteresis and butterfly loops of piezoelectric film substrates: PV (a, b), PD-N (c, d) and PV-N (e, f).

To investigate the potential outputs of the prepared film substrates, potential signals over the films were recorded by oscilloscope in a similar condition of MS-NL in the absence of TC solution. The acquired potential signals are described in Fig. 7. There is nearly no potential output detected over PD film, it is due to that PD substrate does

not possess piezoelectric property. The potentials of PD-N are ranged from -0.2 V to +0.2 V. The possible reason for the low potential output may be that PD substrate without piezoelectric effect, possessing great elastic property, will deform immediately when suffering bending deformation, the stresses and deformations allocated to N powders are very little. PV film generates higher piezoelectric potentials, varying from -0.48 V to +0.48 V. It is ascribed to the piezoelectric effect of PV and its excellent flexibility, which allows it to deform easily and thereby generate piezoelectric potential. Whereas, the piezoelectric potential output over PV-N, ranged from -1.8 V to +1.8 V, is the highest among all the as-prepared film substrates, resulting from the more striking piezoresponses of PV-N than PV and PD-N (Fig. 7). In addition, N powders inside PV bulk serve as stress concentration points and divide PV substrate into plenty of micro-segments, which results in a dramatic improvement on the local deformation of PV and higher piezoelectric potential output. It indicates that the introduction of inorganic ferroelectric N powders into PV flexible substrate is a crucial factor to generate higher piezoelectric potential.

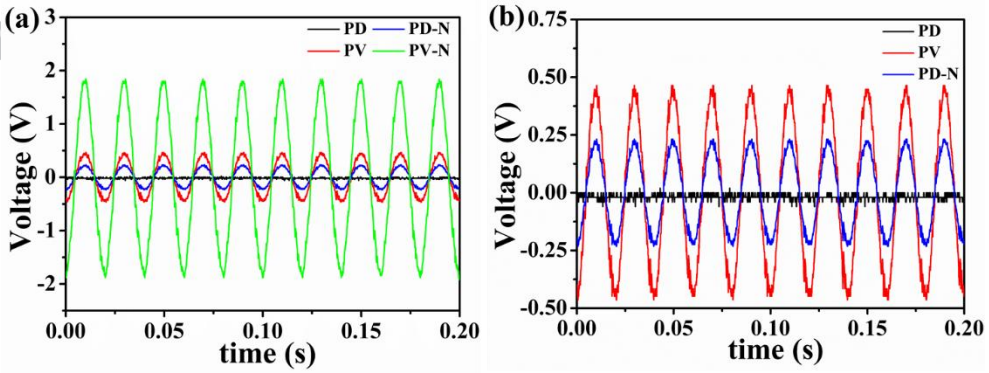

Fig. 7 Piezoelectric potential output signals over PD, PV, PD-N and PV-N film substrates (a), high-precision potential output signals of PD, PV and PD-N (b).

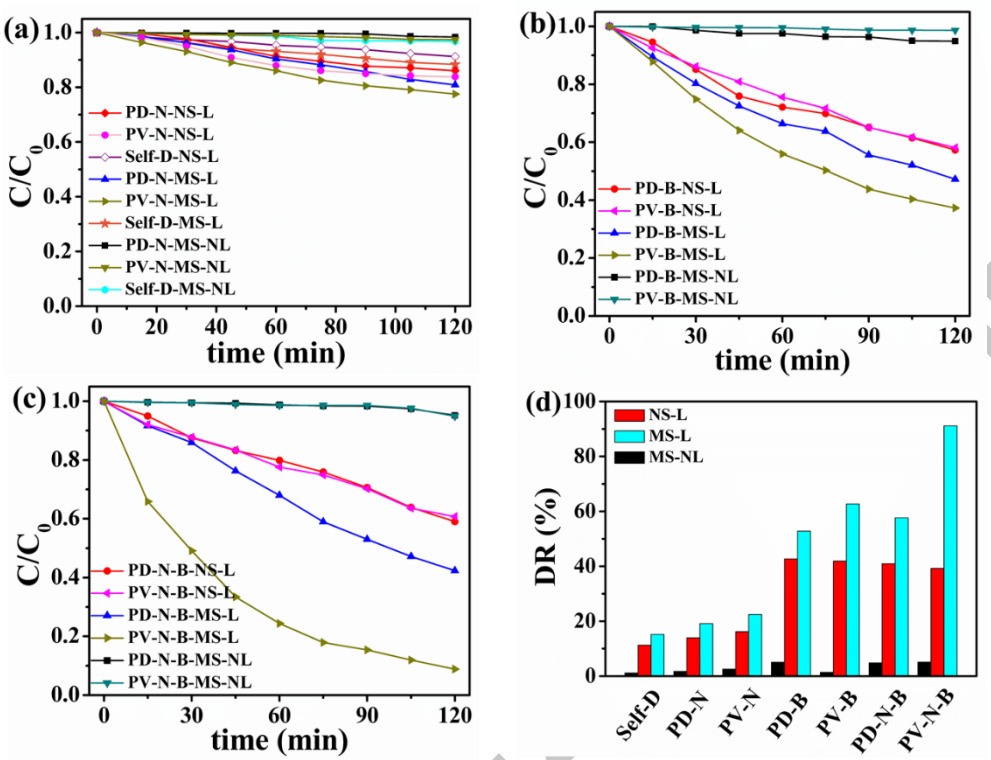

Fig. 8 Catalytic degradation curves of TC (10 mg/L, 100 mL) over the prepared composite films under magnetic stirring in the presence (MS-L) and absence of (MS-NL) light illumination and in the condition of light irradiation with no stirring (NS-L): PD-N, PV-N and the self-degradation of TC (Self-D) (a), PD-B and PV-B (b), PD-N-B and PV-N-B (c) respectively. The degradation efficiency of TC in 120 min (d).

The photocatalytic capability of PD-N, PV-N, PD-B, PV-B, PD-N-B and PV-N-B were characterized under MS-L, NS-L and MS-NL, respectively. The degradation curves of TC are depicted in Fig. 8. The degradations of TC over PD-N and PV-N are very low, less than 20% under MS-L and NS-L, which is similar to the self-degradation of TC, as shown in Fig. 8 (a). It implies that both of PV-N and PD-N samples do not possess photocatalytic activity, though both films are responsive to visible light. Fig. 8 (b) displays that the photocatalytic efficiencies of PV-B and PD-B are 42% and 43% under NS-L, respectively. It indicates the similar contents of B deposited on the surfaces of PV and PD substrates. Compared with NS-L, MS-L improves the TC degradation efficiency over PV-B (63%) and PD-B (53%) by about

1.50 times and 1.26 times, respectively. As Fig. 8 (c) describes, the photocatalytic activity of PV-N-B is dramatically increased by about 2.33 times (from 39% (NS-L) to 91% (MS-L)) with the assistance of MS-L. Nevertheless, the photocatalytic efficiency of PD-N-B is just improved by 1.44 times from 41% (NS-L) to 58% (MS-L), which is much lower than the increases in the photocatalytic activity of PV-N-B.

For clear comparison, the catalytic efficiencies of TC by its self-degradation and over the aforementioned films in 120 min are summarized in Fig. 8 (d). The degradation efficiencies of TC over PV-N and PD-N are in the same level as that introduced by its self-degradation, it indicates that though the prepared N is responsive to visible light, it could not degrade TC. The similar photocatalytic activities among PV-B, PD-B, PV-N-B and PD-N-B under NS-L (approximately 40%), on the one hand, demonstrate that the presence of N does not endow PV-N-B and PD-N-B with higher photocatalytic activity than PV-B and PD-B. On the other hand, it indicates that there are few differences in the amounts of B growing on film substrates PV, PD, PV-N and PD-N. However, the photodegradation efficiency of TC over PV-N-B is much higher than that of PD-B, PV-B and PD-N-B in the condition of MS-L. The catalytic efficiency increases in PV-N-B (~50%) are about 5.0 times, 2.5 times and 2.9 times higher than the counterparts in PD-B (~10%), PV-B (~20%) and PD-N-B (~17%), respectively. Significantly, the sequence of photocatalytic efficiency increases over the prepared photocatalytic composite films (PV-N-B > PV-B> PD-N-B > PD-B) is in the same order of the piezoelectric potential outputs of the film

substrates (PV-N (1.8 V) > PV (0.48 V) > PD-N (0.2 V) > PD (~0 V)). It should be pointed out that the photocatalytic efficiency improvement over PD-B, without piezoelectric potential output, owes to the accelerated mass transfer introduced by magnetic stirring. Importantly, the results suggest that higher piezoelectric potential is more beneficial for photocatalytic performance enhancement.

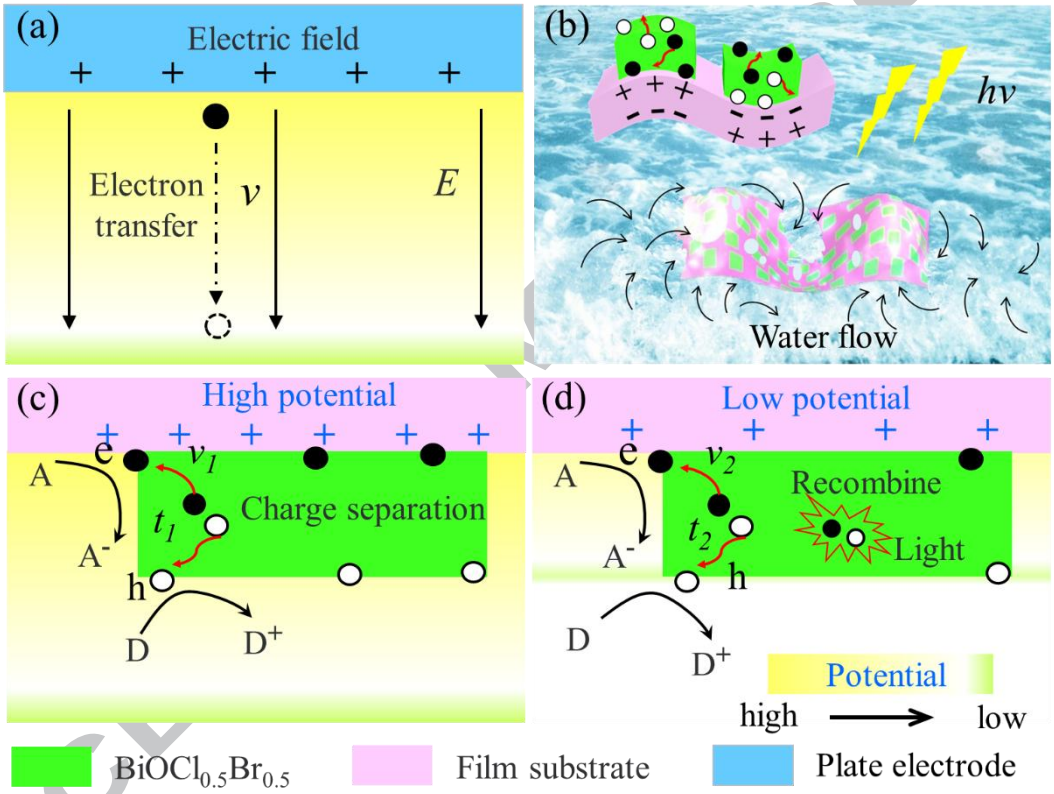

Fig. 9 The mechanism of piezoelectric potential improving photocatalytic activity. Electron accelerates along the direction of electric field E, the transfer velocity of the electron is v (a), flexible composite film deforms as water flows and the photointroduced electrons and holes are generated in the presence of light illumination (b), carries transfer behaviors under high (c) and low (d) potentials. v_1 and v_2 are the carrier migration speed with the assistance of high (c) and low (d) potentials, t_1 and t_2 are the corresponding time for carries to transfer to the surfaces of photocatalyst, respectively.

To distinctly understand the promotive process of piezoelectric potential in photocatalytic activity, a possible mechanism is proposed and illustrated in Fig. 9. As we know, when an electron locates in electric field (Fig. 9 (a)), the electron transfer

behavior will be sped up by electric field based on fundamental physical theories and the transfer velocity of electron shows a positive correlation with electric field intensity. Similarly, the transfer behavior of photogenerated electrons of photocatalyst will also be influenced by electric field. Therefore, when PV-B, PD-N-B or PV-N-B films are irradiated with light illumination in flowing water (Fig. 9 (b)), photogenerated electrons and holes of B will be excited, the film will deform as water flows and thereby the piezoelectric potential of film substrates PV, PD-N or PV-N will be generated. As Fig. 9 (c) illustrates, under higher potential outputs over PV-N substrate, almost all the electrons and holes move oppositely to the surfaces of B with a higher speed of v_1, in which process it takes carriers t_1 to arrive at the surfaces and participate in photocatalytic reactions. In the condition of lower potential over PV or PD-N substrates, depicted in Fig. 9 (d), many carries transfer to the surfaces of photocatalyst in t_2 with a speed of v_2, while some carries may recombine together before taking part in photocatalytic reactions owing to small driven force. It can be inferred that under higher piezoelectric field intensity of PV-N substrate, v_1 is higher than v_2 and the corresponding time t_1 is shorter than t_2. Thus, the charge recombination probability of PV-N-B is lower than that of PV-B and PD-N-B, which results in flexible composite film PV-N-B with much higher photocatalytic efficiency than that of PV-B and PD-N-B. Importantly, it may be concluded that the higher piezoelectric potential is more favorable to boost up photocatalytic property by obvious accelerating carrier transfer and prohibiting charge recombination.

To clarify the photodegradation pathway of TC over flexible composite film PV-N-B, the intermediates produced in the photodegradation reaction process were analyzed with HPLC and LC-MS, respectively. A prominent ion with m/z=445 is clearly observed, which corresponds to the characteristic peak of TC. The intensity of TC peak at m/z=445 becomes weaker and other peaks with m/z of 417, 401, 384, 292, 245, 161, 147 and 128 appear gradually with photocatalytic reaction time. Based on the experimental results and reported studies, the possible pathways of TC photocatalytic degradation are proposed, illustrated in Fig. 10. The intermediates are mainly generated through the loss of functional group(s) and the open-ring reactions [3, 38-42]. At last, the intermediate products would be degraded to CO_2, H_2O and some other small inorganic molecular materials.

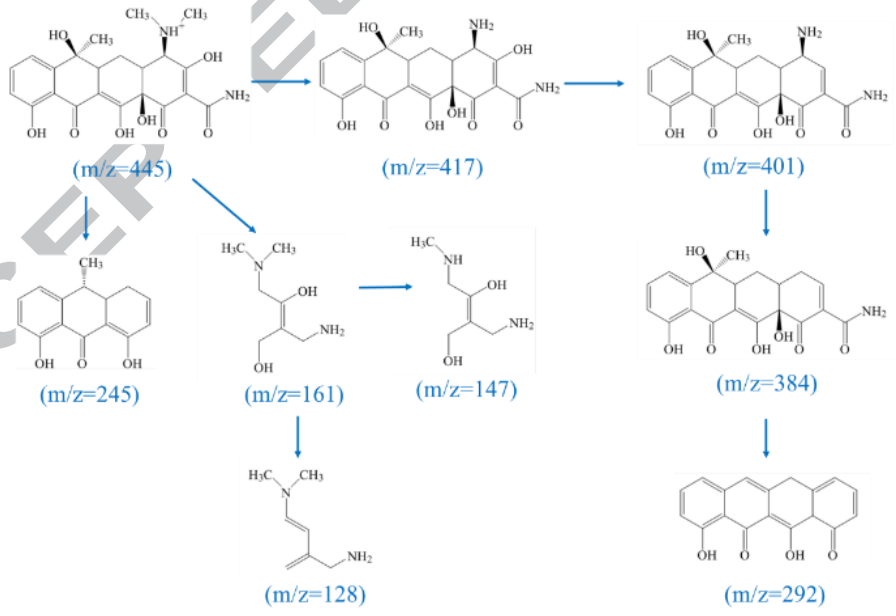

Fig. 10 Proposed degradation pathways for the photocatalytic degradation of TC over flexible composite film PV-N-B under MS-L.

The active species trapping experiments were performed to figure out the decisive species, which play a crucial role in the photocatalytic degradation of TC. The

acquired degradation curves of TC over flexible composite film PV-N-B in the presence and absence of scavengers are depicted in Fig. 11. 91.1% of TC is degraded by PV-N-B in 120 min without any scavenger. The attendances of IPA and TEA, added to trap hydroxyl radicals and photoexcited holes respectively, do not make a big difference in the photocatalytic degradation efficiencies of TC. On the contrary, with hexavalent chromium (Cr) and BQ injected into the solution to respectively trap photoinduced electrons and superoxide radicals, the photodegradation activities are obviously inhibited, decreasing to 37.1% and 41.2%, respectively. It is well known that superoxide radicals are the reduction products of photogenerated electrons and oxygen in the photocatalytic system. It implies that when photoinduced electrons are trapped by Cr, the production of superoxide radicals will be halted. It indicates that all the catalytic reactions superoxide radicals participating in will get suspended. Thus, it can be deduced that Cr impedes the photodegradation of TC by trapping photogenerated electrons to control the production of superoxide radicals. Therefore, the superoxide radicals are the major reactive species for the degradation of TC over PV-N-B.

The photocatalytic reusability and durability of flexible composite film PV-N-B were studied by cyclic experiments for five times under MS-L. Fig. 12 suggests that the photocatalytic activity of PV-N-B still maintains well after five successive runs. This result manifests the great photocatalytic stability of PV-N-B, which is also verified by the little difference between the SEM images of PV-N-B film before and after photocatalytic characterization (Fig. S4). Moreover, the degradation rate over

each run is almost the same, indicating that the photocatalytic activity is accelerated throughout the whole cyclic degradation process. The stable photocatalytic activity improvements also imply the great piezoelectric durability of PV-N substrate. Therefore, flexible composite film PV-N-B, possessing superb capability in converting flowing water energy into piezoelectric potential and excellent photocatalytic performance, is a promising candidate to bring the environmental containments under control.

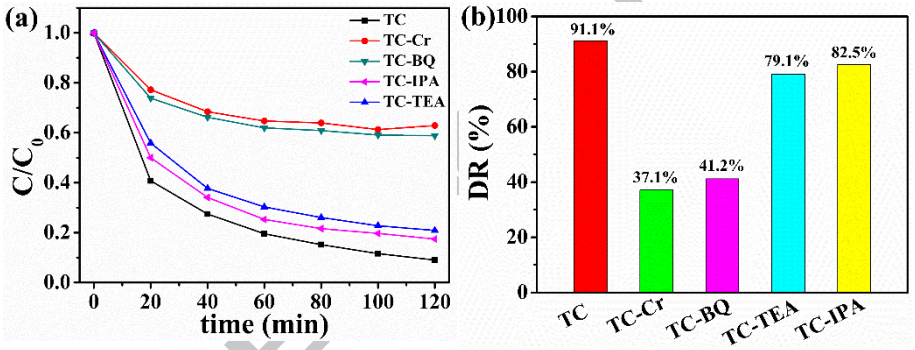

Fig. 11 The photodegradation curves of TC (10 mg/L, 100 mL) over flexible composite film PV-N-B film with and without scavenger under MS-L (a), the degradation efficiency of TC in 120 min (b).

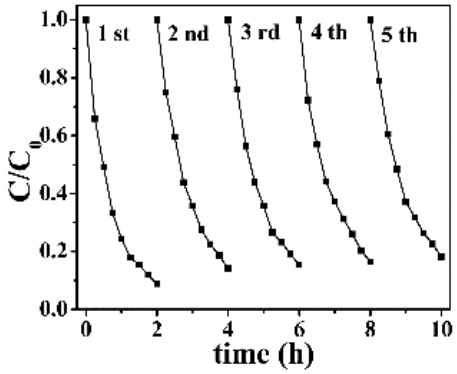

Fig. 12 The cyclic photodegradation curves of TC (10 mg/L, 100 mL) over flexible composite film PV-N-B under MS-L.

In addition, PV-N-B composite films contained different amounts of N powders

(weight ratio between N and PV ranged from 0.25:1 to 1.5:1) were prepared as well to investigate the effect of N contents in film substrate on the photocatalytic activity of composite film. Fig. S5 shows that the photocatalytic efficiency of PV-N-B with the weight ratio of 1:1 between PV and N is the highest, which is the result of the interaction between the piezoelectric potential output and flexibility over PV-N substrate. Moreover, to explore the influence of the morphology of N on the piezoelectric and photocatalytic property over composite film, N nanorod (Nr) and N nanofiber with nanosphere (Nfs) powders (Fig. S6 and Fig. S7) were prepared to fabricate PV-Nr-B and PV-Nfs-B films. The photocatalytic performance of PV-Nr-B and PV-Nfs-B were evaluated by degrading TC under MS-L and NS-L (Fig. S8), respectively. It suggests that the photocatalytic activity of PV-N-B is higher than that of PV-Nr-B and PV-Nfs-B films, which is due to the better piezoelectric property (Fig. S9) and higher piezoelectric potential output (Fig. S10) of PV-N substrate. This result once again indicates that higher piezoelectric potential possesses more advantages in photocatalytic performance enhancement.

4. Conclusions

In summary, flowing water energy has been converted to piezoelectric potential by a new type of flexible composite film PV-N-B, which strikingly boosts its photocatalytic capability on the degradation of TC by 2.33 times. It may be ascribed to the accelerated carrier transfer and the suppressed charge recombination driven by piezoelectric potential. Importantly, it indicates that the higher piezoelectric potential is more favorable for photocatalytic performance enhancement. Furthermore, the

photocatalytic degradation intermediates of TC over PV-N-B could be finally degraded to some small molecular materials through the loss of functional group(s) and the open-ring reactions. It verifies that the superoxide radicals are the major reactive species for the degradation of TC over PV-N-B. Our present work constructs an efficient flexible composite film, with great capability in coupling flowing water energy and solar energy, resulting in promoted spatial directed charge separation and dramatically enhanced photocatalytic performance, which provides great potential to control or eliminate environmental containments.

Acknowledgements

The authors are particularly grateful to Prof. Hong Liu from Shandong University in Shandong Province for the assistance on PFM imaging. Financial support from National Natural Science Foundation of China (No. 51502143), Natural Science Foundation of Jiangsu Province (No. BK20150919), Qing Lan Project, Six Talent Peaks Project in Jiangsu Province (No. XCL-029), Jiangsu Province Postdoctoral Fund (No. 1302096C), Key University Science Research Project of Jiangsu Province (No.15KJB430022) and Priority Academic Program Development of the Jiangsu Higher Education Institutions (PAPD) is gratefully acknowledged.

References

[1] M. Yan, Y. Hua, F. Zhu, W. Gu, J. Jiang, H. Shen, W. Shi, Fabrication of nitrogen doped graphene quantum dots-BiOI/MnNb2O6 p-n junction photocatalysts with enhanced visible light efficiency in photocatalytic degradation of antibiotics, Appl. Catal. B: Environ. 202 (2017) 518-527.

[2] J.L. Martinez, Environmental pollution by antibiotics and by antibiotic resistance determinants, Environ. Pollut. 157 (2009) 2893-2902.

[3] M. Yan, Y. Hua, F. Zhu, W. Gu, J. Jiang, H. Shen, W. Shi, Fabrication of nitrogen doped graphene quantum dots-BiOI/MnNb2O6 p-n junction photocatalysts with enhanced visible light efficiency in photocatalytic degradation of antibiotics, Appl. Catal. B: Environ. 202 (2017) 518-527.

[4] Y. Ding, G. Zhang, X. Wang, L. Zhu, H. Tang, Chemical and photocatalytic oxidative degradation of carbamazepine by using metastable Bi3+ self-doped NaBiO3 nanosheets as a bifunctional material, Appl. Catal. B: Environ. 202 (2017) 528-538.

[5] P. Singh, B. Priya, P. Shandilya, P. Raizada, N. Singh, B. Pare, S.B. Jonnalagadda, Photocatalytic mineralization of antibiotics using 60%WO3/BiOCl stacked to graphene sand composite and chitosan, Arab. J. Chem. (2016).

[6] S. Fukahori, T. Fujiwara, Photocatalytic decomposition behavior and reaction pathway of sulfamethazine antibiotic using TiO2, J. Environ. Manage. 157 (2015) 103-110.

[7] X. Zhang, R. Li, M. Jia, S. Wang, Y. Huang, C. Chen, Degradation of ciprofloxacin in aqueous bismuth oxybromide (BiOBr) suspensions under visible light irradiation: A direct hole oxidation pathway, Chem. Eng. J. 274 (2015) 290-297.

[8] Y. Lai, M. Meng, Y. Yu, X. Wang, T. Ding, Photoluminescence and photocatalysis of the flower-like nano-ZnO photocatalysts prepared by a facile hydrothermal method with or without ultrasonic assistance, Appl. Catal. B: Environ. 105 (2011) 335-345.

[9] J.B. Joo, I. Lee, M. Dahl, G.D. Moon, F. Zaera, Y. Yin, Controllable Synthesis of Mesoporous TiO2 Hollow Shells: Toward an Efficient Photocatalyst, Adv. Funct. Mater. 23 (2013) 4246-4254.

[10] H. Li, Y. Sang, S. Chang, X. Huang, Y. Zhang, R. Yang, H. Jiang, H. Liu, Z.L. Wang, Enhanced Ferroelectric-Nanocrystal-Based Hybrid Photocatalysis by Ultrasonic-Wave-Generated Piezophototronic Effect, Nano Lett. 15 (2015) 2372-2379.

[11] B. Dai, C. Lu, J. Kou, Z. Xu, F. Wang, Photocatalytic performance of PMN-PT@TiO2 highly enhanced by alternative spatial electric field induced charge separation effect, J. Alloy. Compd. (2017) 988-995.

[12] B. Dai, L. Zhang, H. Huang, C. Lu, J. Kou, Z. Xu, Photocatalysis of composite film PDMS-PMN-PT@TiO2 greatly improved via spatial electric field, Appl. Surf. Sci. (2017) 9-14.

[13] X. Xue, W. Zang, P. Deng, Q. Wang, L. Xing, Y. Zhang, Z.L. Wang, Piezo-potential enhanced photocatalytic degradation of organic dye using ZnO nanowires, Nano Energy 13 (2015) 414-422.

[14] Cong Sun, Yongming Fu, Qiang Wang, Lili Xing, B. Liu, X. Xue, Ultrafast piezo-photocatalytic degradation of organic pollutions by Ag2O/tetrapod-ZnO nanostructures under ultrasonic/UV exposure, RSC Adv. 6 (2016) 87446 – 87453.

[15] X. Guo, Y. Fu, D. Hong, B. Yu, H. He, Q. Wang, L. Xing, X. Xue, High-efficiency sono-solar-induced degradation of organic dye by the piezophototronic/photocatalytic coupling effect of FeS/ZnO nanoarrays, Nanotechnology 27 (2016) 375704.

[16] D. Hong, W. Zang, X. Guo, Y. Fu, H. He, J. Sun, L. Xing, B. Liu, X. Xue, High Piezo-photocatalytic Efficiency of CuS/ZnO Nanowires Using Both Solar and Mechanical Energy for Degrading Organic Dye, ACS Appl. Mater. Inter. 8 (2016) 21302-21314.

[17] Y. Xu, P. Chen, J. Zhang, S. Xie, F. Wan, J. Deng, X. Cheng, Y. Hu, M. Liao, B. Wang, X. Sun, H. Peng, A One-Dimensional Fluidic Nanogenerator with a High Power Conversion Efficiency, Angew. Chem. Int. Edit. 56 (2017) 1-7.

[18] Yuelei Sia, Shuang Cao, Zhijiao Wu, Yinglu Ji, Yang Mi, Xiaochun Wu, X. Liu, Lingyu Piaoa, The effect of directed photogenerated carrier separation on photocatalytic hydrogen production, Nano Energy 41 (2017) 488–493.

[19] G. Liu, G. Zhao, W. Zhou, Y. Liu, H. Pang, H. Zhang, D. Hao, X. Meng, P. Li, T. Kako, J. Ye, In Situ Bond Modulation of Graphitic Carbon Nitride to Construct p-n Homojunctions for Enhanced Photocatalytic Hydrogen Production, Adv. Funct. Mater. 26 (2016) 6822-6829.

[20] X. Yu, X. Han, Z. Zhao, J. Zhang, W. Guo, C. Pan, A. Li, H. Liu, Z. Lin Wang, Hierarchical TiO2 nanowire/graphite fiber photoelectrocatalysis setup powered by a wind-driven nanogenerator: A highly efficient photoelectrocatalytic device entirely based on renewable energy, Nano Energy 11 (2015) 19-27.

[21] S. Lee, S. Bae, L. Lin, Y. Yang, C. Park, S. Kim, S.N. Cha, H. Kim, Y.J. Park, Z.L. Wang, Super-Flexible Nanogenerator for Energy Harvesting from Gentle Wind and as an Active Deformation Sensor, Adv. Funct. Mater. 23 (2013) 2445-2449.

[22] M.X. Li, L.P. Ricard, J. Underschultz, B.M. Freifeld, Reducing operational costs of CO2 sequestration through geothermal energy integration, Int. J. Greenh. Gas Con. 44 (2016) 238-248.

[23] H. Ren, M. Tang, B. Guan, K. Wang, J. Yang, F. Wang, M. Wang, J. Shan, Z. Chen, D. Wei, H. Peng, Z. Liu, Hierarchical Graphene Foam for Efficient Omnidirectional Solar-Thermal Energy Conversion, Adv. Mater. 29 (2017) 1702590.

[24] X.D. Xie, Q. Wang, N. Wu, Potential of a piezoelectric energy harvester from sea waves, J. Sound Vib. 333 (2014) 1421-1429.

[25] X. Lu, H. Qu, M. Skorobogatiy, Piezoelectric Micro- and Nanostructured Fibers Fabricated from Thermoplastic Nanocomposites Using a Fiber Drawing Technique: Comparative Study and Potential Applications, ACS Nano 11 (2017) 2103-2114.

[26] S.K. Ghosh, D. Mandal, High-performance bio-piezoelectric nanogenerator made with fish scale, Appl. Phys. Lett. 109 (2016) 103701.

[27] Y. Mao, P. Zhao, G. McConohy, H. Yang, Y. Tong, X. Wang, Sponge-Like Piezoelectric Polymer Films for Scalable and Integratable Nanogenerators and Self-Powered Electronic Systems, Adv. Energy Mater. 4 (2014) 1301624.

[28] P. Talemi, M. Delaigue, P. Murphy, M. Fabretto, Flexible Polymer-on-Polymer Architecture for Piezo/Pyroelectric Energy Harvesting, ACS Appl. Mater. Inter. 7 (2015) 8465-8471.

[29] J. Song, G. Zhao, B. Li, J. Wang, Design optimization of PVDF-based piezoelectric energy harvesters, Heliyon 3 (2017) e00377.

[30] R. Tian, Q. Xu, C. Lu, X. Duan, R. Xiong, Spontaneous polarization switching and piezoelectric enhancement of PVDF through strong hydrogen bonds induced by layered double hydroxides, Chem. Commun. 53 (2017) 7933-7936.

[31] Y. Kim, Y. Xie, X. Wen, S. Wang, S.J. Kim, H. Song, Z.L. Wang, Highly porous piezoelectric PVDF membrane as effective lithium ion transfer channels for enhanced self-charging power cell, Nano Energy 14 (2015) 77-86.

[32] Baoying Dai, Hengming Huang, Wei Wang, Yukai Chen, Chunhua Lu, Jiahui Kou, Lianzhou Wang, Fulei Wang, Z. Xu, Greatly enhanced photocatalytic activity by organic flexible piezoelectric PVDF induced spatial electric field, Catal. Sci. Technol. 7 (2017) 5594–5601.

[33] Y. Zhao, Q. Liao, G. Zhang, Z. Zhang, Q. Liang, X. Liao, Y. Zhang, High output piezoelectric nanocomposite generators composed of oriented BaTiO3 NPs@PVDF, Nano Energy 11 (2015) 719-727.

[34] Z. Pi, J. Zhang, C. Wen, Z. Zhang, D. Wu, Flexible piezoelectric nanogenerator made of poly(vinylidenefluoride-co-trifluoroethylene) (PVDF-TrFE) thin film, Nano Energy 7 (2014) 33-41.

[35] Y. Kim, Y. Xie, X. Wen, S. Wang, S.J. Kim, H. Song, Z.L. Wang, Highly porous piezoelectric PVDF membrane as effective lithium ion transfer channels for enhanced self-charging power cell, Nano Energy 14 (2015) 77-86.

[36] D. Zhou, Y. Zhou, Y. Tian, Y. Tu, G. Zheng, H. Gu, Structure and Piezoelectric Properties of

Lead-Free Na0.5Bi0.5TiO3 Nanofibers Synthesized by Electrospinning, J. Mater. Sci. Technol. 31 (2015) 1181-1185.

[37] X. Zhou, C. Jiang, C. Chen, H. Luo, K. Zhou, D. Zhang, Morphology control and piezoelectric response of Na0.5Bi0.5TiO3 synthesized via a hydrothermal method, CrystEngComm (2016) 1302-1310.

[38] B. Gao, S. Dong, J. Liu, L. Liu, Q. Feng, N. Tan, T. Liu, L. Bo, L. Wang, Identification of intermediates and transformation pathways derived from photocatalytic degradation of five antibiotics on ZnIn2S4, Chem. Eng. J. 304 (2016) 826-840.

[39] M. Cao, P. Wang, Y. Ao, C. Wang, J. Hou, J. Qian, Visible light activated photocatalytic degradation of tetracycline by a magnetically separable composite photocatalyst: Graphene oxide/magnetite/cerium-doped titania, J. Colloid Interf. Sci. 467 (2016) 129-139.

[40] J. Niu, S. Ding, L. Zhang, J. Zhao, C. Feng, Visible-light-mediated Sr-Bi2O3 photocatalysis of tetracycline: Kinetics, mechanisms and toxicity assessment, Chemosphere 93 (2013) 1-8.

[41] X. Wang, J. Jia, Y. Wang, Combination of photocatalysis with hydrodynamic cavitation for degradation of tetracycline, Chem. Eng. J. 315 (2017) 274-282.

[42] D. He, Y. Sun, S. Li, J. Feng, Decomposition of tetracycline in aqueous solution by corona discharge plasma combined with a Bi2MoO6 nanocatalyst, J. Chem. Technol. Biot. 90 (2015) 2249-2256.

Graphical Abstract

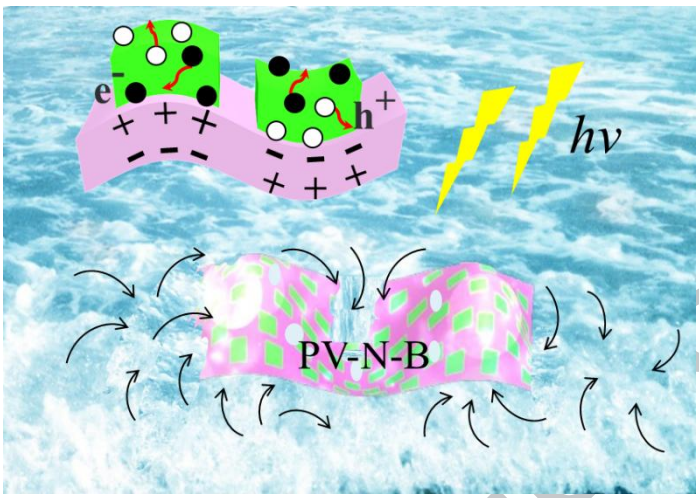

Highlights

1. The generation of piezoelectric potential in the designed flexible photocatalyst film PV-N-B can be driven by mild flowing water energy, and thereby boosts its photocatalytic activity by 2.33 times.

2. It demonstrates that higher piezoelectric potential is more beneficial for improving photocatalytic performance.

3. The role of piezoelectric potential in the enhancement of photocatalytic activity has been discussed in detail.

4. The photocatalytic degradation intermediates of tetracycline over PV-N-B were detected and the possible photodegradation pathway has been reasonably proposed.

5. The generated active species on PV-N-B during the degradation process of tetracycline have been studied.